Journal of Materials Chemistry C

ROYAL SOCIETY OF CHEMISTRY

PAPER

View Article Online
View Journal | View Issue

Cite this: J. Mater. Chem. C, 2022, 10, 1220

Eu^{2+} emission from thermally coupled levels – new frontiers for ultrasensitive luminescence thermometry†

Małgorzata Sójka, [a] Marcin Runowski, *[b] Teng Zheng, [b] Andrii Shyichuk, [a] Dagmara Kulesza, [a] Eugeniusz Zych *[a] and Stefan Lis [b]

Designing luminescent thermometers operating in a broad *T*-range, spanning hundreds of degrees, presenting high thermal sensitivity and good resolution is one of the greatest challenges in the field. In this paper, we present $SrB_4O_7:Eu^{2+}$, a novel luminescent thermometer, operating in the *T*-range of 11–600 K and presenting unprecedentedly high relative thermal sensitivity, *i.e.*, up to ≈10.5%/K and ≈22.6%/K, using either Eu^{2+} luminescence decay time or intensity ratio as thermometric parameters, respectively. Such good performance classifies the $SrB_4O_7:Eu^{2+}$ phosphor as the most sensitive inorganic luminescent thermometer ever reported. The temperature dependences of both luminescence intensity ratios and the emission decay time result from the same physical effect, *i.e.*, thermal coupling of the lowest $5d_1$ excited level of Eu^{2+} and the $^6P_{7/2}$ excited level of the $4f^7$ configuration of the dopant. The latter one is located ≈130 cm^{-1} below the $5d_1$. Such a strong coupling changes the contribution of the emission from the two levels, in response to the temperature change, but without any significant luminescence thermal quenching. This beneficial situation allows measuring spectra with a high signal-to-noise ratio, which lowers the uncertainty of the temperature measurement (improves resolution) in the whole operating *T*-range. The $SrB_4O_7:Eu^{2+}$ material offers a broad operating *T*-range, as well as unprecedentedly high relative thermal sensitivity and low uncertainty of the temperature measurement.

Received 18th October 2021,
Accepted 23rd November 2021

DOI: 10.1039/d1tc05022b

rsc.li/materials-c

1. Introduction

Developing highly sensitive luminescent thermometers is a challenging task. When the required/expected temperature range to be detected exceeds several hundred degrees, the design of such thermometers becomes even more demanding.[1,2] As noted in ref. 3 a wide measuring range and high sensitivity of luminescent thermometers are slightly opposite requirements. Hence, one cannot expect that the high relative thermal sensitivity may be retained over the range of hundreds of degrees. However, it is conceivable a luminescent thermometer can operate over such a wide *T*-range, offering simultaneously high thermal sensitivity in the whole *T*-range, due to the use of a multi-parameter (multi-mode) sensing strategy.[4–6] Such characteristics of a luminescent thermometer may be useful in various practical applications.

Luminescence of Eu^{2+} typically consists of broadband emission resulting from its 5d → 4f transition. Fig. 1a presents the situation when the 5d level has lower energy than the $^6P_{7/2}$ one and then only the 5d → 4f emission may occur. This situation is not attractive from the point of view of

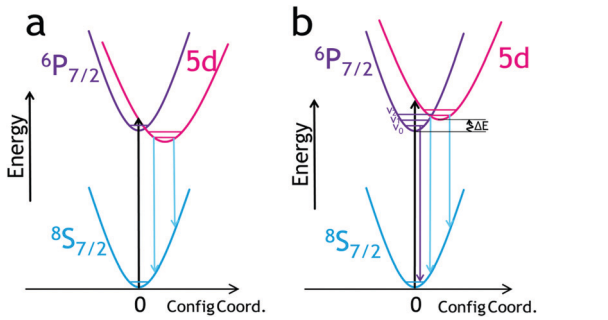

Fig. 1 Schematic diagram of the energy levels of the Eu^{2+} ion. In (a), the 5d level is positioned below the $^6P_{7/2}$ one, which precludes the $^6P_{7/2}$ → $^8S_{7/2}$ radiative relaxation, and only the 5d → 4f luminescence occurs. In (b), both narrow and broadbands corresponding to the $^6P_{7/2}$ → $^8S_{7/2}$ and 5d → $4f(^8S_{7/2})$ transitions, respectively, are possible, and their relative intensities (populations) are mainly governed by thermal coupling (situation valid for the $SrB_4O_7:Eu^{2+}$ system).

[a] University of Wroclaw, Faculty of Chemistry 14. F. Joliot-Curie Street, Wroclaw 50-383, Poland. E-mail: eugeniusz.zych@chem.uni.wroc.pl
[b] Adam Mickiewicz University, Faculty of Chemistry Uniwersytetu Poznańskiego 8, Poznań 61-614, Poland. E-mail: runowski@amu.edu.pl

† Electronic supplementary information (ESI) available. See DOI: 10.1039/d1tc05022b

luminescence thermometry. Yet, Eu^{2+} may also generate photons as a consequence of the 4f → 4f transition, when the $^6P_{7/2}$ excited manifold of the $4f^7$ configuration is located below the lowest-energy $5d_1$ level of the ion (see Fig. 1b). While generally uncommon, in some hosts such 4f → 4f emission of Eu^{2+} occurs, presenting the characteristic narrow lines, associated with the intra-configurational $^6P_{7/2} \rightarrow {}^8S_{7/2}$ transition.[7,8] For the reasons discussed below, it may occur at rather low temperature values (cryogenic *T*-range). If the $^6P_{7/2}$ level is located below the $5d_1$ one, both levels may be thermally-coupled. Since the lifetime of the $^6P_{7/2}$ level is typically much longer (forbidden f–f transitions) than the lifetime of the 5d level (parity-allowed d–f transitions), once the coupling occurs, the 5d → 4f transition contributes to the emission effectively. The luminescence character may then change upon the increase of temperature, from the entirely intra-configurational 4f → 4f transition (narrow lines) to the inter-configurational 5d → 4f one (broadband).[8]

In such a situation, with increasing temperature, not only does the luminescence spectrum change significantly but also the emission decay time shortens, as the contribution of the parity-allowed 5d → 4f transition increases.[10] Consequently, both the shape of the luminescence spectrum and the decay time of the emission may be potentially useful for thermometric applications. We shall present in this paper that such characteristics of Eu^{2+} luminescence may lead to unprecedentedly high relative thermal sensitivity of an optical thermometer, combined with a very broad operating *T*-range. Importantly, we consider the harmonization of both effects within a single inorganic compound is a significant achievement with the prospect of searching for other phosphors showing similar effects, and possibly offering even better thermometric performance.

The SrB_4O_7 host lattice is an excellent candidate for activation with Ln^{2+} ions. It has been shown that the tetrahedral structure of the BO_4 groups stabilizes such dopants effectively, even in an oxidizing atmosphere and at high temperatures.[11,12] The reducing capability of the host has been already demonstrated for Sm^{2+},[13,14] Yb^{2+},[15] Tm^{2+},[16] Nd^{2+},[17] and even Bi^{2+}[18,19] ions, despite their lower reduction potential, compared to Eu^{3+}. The stability of Eu^{2+} in the SrB_4O_7 host was proven many years ago.[8]

Recently, we have presented the benefits of applying the 5d → 4f emissions of Pr^{3+} and Tm^{2+} in luminescence thermometry, showing that the use of their inter-configurational transitions greatly enhances the relative thermal sensitivity of such thermometers.[20–24] Now, we turn our attention to the Eu^{2+} luminescence and its possible utility in the optical determination of temperature. The emission intensity of this ion is often strong, due to the broadband parity-allowed 4f → 5d excitation transition, that can be easily realized using standard light sources, which also widens the variety of potential applications.

Until now, a few strategies to exploit Eu^{2+} luminescence as an optical thermometer were employed. These involved the ratio of the Eu^{2+}/Eu^{3+} emission intensities,[25,26] the ratio of emission bands from Eu^{2+} occupying different sites of the host lattice,[27,28] the rate of energy transfer between Eu^{2+} and other d- or f-block elements.[29] Yet, to the best of our knowledge, there are no reports on the use of the Eu^{2+} 5d → 4f and 4f → 4f transition intensity ratio as a thermometric parameter. Detailed analysis of the fundamental research results on SrB_4O_7:Eu^{2+}[8] led us to the conclusion that this phosphor may offer particularly interesting thermometric properties. In this paper, we explore the idea focusing both on the SrB_4O_7:Eu^{2+} luminescence spectra and the emission kinetics. We show that SrB_4O_7:Eu^{2+} may work as a dual-mode ratiometric luminescent thermometer, using the luminescence intensity ratio (LIR) of its emission features and decay time of its luminescence. Moreover, we prove that it can operate in a broad *T*-range and show unprecedentedly high relative thermal sensitivity in cryo-range, whichever of the two modes is exploited.

2. Experimental

2.1. Synthesis

A powder SrB_4O_7:Eu^{2+} (3 mol%) was synthesized *via* a conventional solid-state (ceramic) method. $SrCO_3$ (Sigma-Aldrich, 99.9%), H_3BO_3 (Chempur, p.a.), Eu_2O_3 (Stanford Materials, 99.99%) were the starting materials. The stoichiometric mixture of the reagents (with 5 mol% excess of H_3BO_3) was thoughtfully ground in an agate mortar with some acetone as a wetting medium. After natural drying, the mixture was transferred into a porcelain crucible covered with a lid and was heated in a furnace for 5 h at 700 °C in air. After cooling down, the powder was ground again and heat-treated for 5 h at 850 °C twice, with an intermediate grinding. It was crucial to cover the crucible with a lid to preclude the evaporation of B_2O_3 from the reacting mixture and limit the oxygen flow.

2.2. Characterization

Powder X-ray diffraction pattern (XRD) was recorded using a Bruker D8 Advance diffractometer. The measurement was performed in the 2θ range of 10–60°, using Cu Ka_1 radiation (λ = 1.5406 Å) with the counting time 0.2 s and the step 0.008°. The reference pattern was taken from Inorganic Crystal Structure Database (ICSD, #14383). The morphology of the sample was analyzed using a Hitachi S-3400N scanning electron microscope (SEM). Photoluminescence (PL), PL excitation spectra (PLE), and luminescence decay (DEC) traces were recorded in the 11–600 K temperature range, with FLS1000 Fluorescence Spectrometer from Edinburgh Instruments Ltd. For PL and PLE measurements a 450 W continuous xenon arc lamp was used as the excitation source, while for DEC traces a 60 W Xe pulse lamp was employed. The sample was mounted on a copper holder in a closed-cycle helium cryostat from Lake Shore Cryotronics, using Silver Adhesive 503 glue from Electron Microscopy Sciences. TMS302-X double grating excitation and emission monochromators of 325 mm focal lengths were used, and the luminescence signal was recorded with a Hamamatsu R928P high-gain photomultiplier detector, thermoelectrically cooled to −22 °C. The excitation spectra were corrected for the incident light intensity and the emission spectra were corrected for the spectral sensitivity of the recording system.

3. Results

3.1. Structural and morphological properties.

Fig. 2a–c presents the results of the structural and morphological characterization of the obtained powder phosphor. The measured XRD diffractogram matches perfectly with the ICSD #14383 reference pattern of SrB_4O_7, proving the expected orthorhombic structure ($P2_1nm$) of the synthesized phosphor material. In SrB_4O_7 there is only one Sr^{2+} cationic site with C_s point symmetry, and Eu^{2+} obviously enters this position. Representative SEM images of the synthesized phosphor material are presented in Fig. 2b and c. The grains have a narrow size distribution and show an elongated shape with about 1 μm length and about 100–150 nm thickness.

3.2. Photoluminescence properties

Fig. 3a presents the PLE spectra of Eu^{2+} luminescence monitored at 367.2 nm and recorded at 11 and 300 K. Fig. 3b shows the PL spectra recorded at the same temperature values, under 300 nm excitation. A detailed analysis of the luminescence spectroscopy of the SrB_4O_7:Eu^{2+} system, including assignment of the observed lines, has already been presented by Meijerink *et al.*[8] Here, we only discuss the temperature-dependent properties, important for the thermometric analysis presented below. The PLE spectra (Fig. 3a) consist of two broad overlapping bands covering roughly 240–280 nm and 280–360 nm ranges. Both bands are assigned to the inter-configurational $4f^7 \rightarrow 4f^65d^1$ transitions. In the spectrum recorded at 11 K, numerous vibronic features can be observed at the low-energy part of the spectrum. The PL spectrum at low-temperature (Fig. 3b) reveals a strong sharp line of the $^6P_{7/2} \rightarrow {}^8S_{7/2}$ (4f → 4f) transition and a well-resolved vibrational structure at its longer wavelengths/lower energy side. The PL spectrum changes significantly when the temperature increases. A broad PL band is observed at 300 K. It originates from the inter-configurational $4f^65d^1 \rightarrow 4f^7(^8S_{7/2})$ transition. Similarly, a significant change of the PL spectrum with temperature was observed in $SrAl_{12}O_{19}$:Eu^{2+}.[30] The onset of the broadband is blue-shifted in respect to the main $^6P_{7/2} \rightarrow {}^8S_{7/2}$ line, indicating that the energetically lowest (emitting) $5d_1$ level is located above the $^6P_{7/2}$ excited level of the $4f^7$ configuration of Eu^{2+}, as discussed in the Introduction part and presented in Fig. 1b. The reason for such location of energy levels in the SrB_4O_7:Eu^{2+} material is the high coordination number (CN = 9) of the Eu^{2+}/Sr^{2+}, which makes the crystal field splitting of the 5d configuration fairly low.[7,9] Additionally, the low covalency of the bonds shifts the $4f^65d^1$ configuration to a higher energy region. Solarz *et al.* proved a weak crystal field splitting for Sm^{2+} in the SrB_4O_7 host lattice, as well.[31] The position of the 5d → 4f luminescence band of Eu^{2+} depends greatly on the host lattice properties. It may vary from 367 nm in SrB_4O_7:Eu^{2+} (Fig. 3b), up to even 850 nm in $Ca_3Sc_2Si_3O_{12}$:Eu^{2+}.[32]

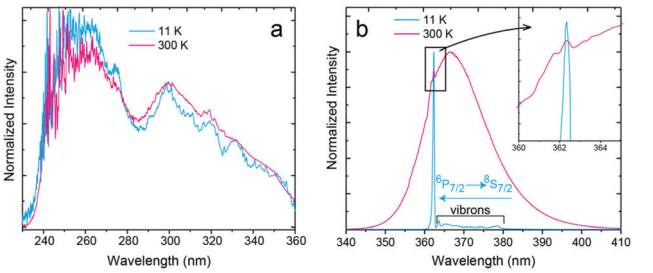

Fig. 3 (a) PLE and PL spectra of SrB_4O_7:Eu^{2+} microparticles. The PLE spectrum was monitored at 367.2 nm and recorded at 11 and 300 K. (b) PL spectra recorded at 11 K and 300 K excited at 300 nm. In-depth analysis of the ZPL lines and vibronic transitions was presented in ref. 8.

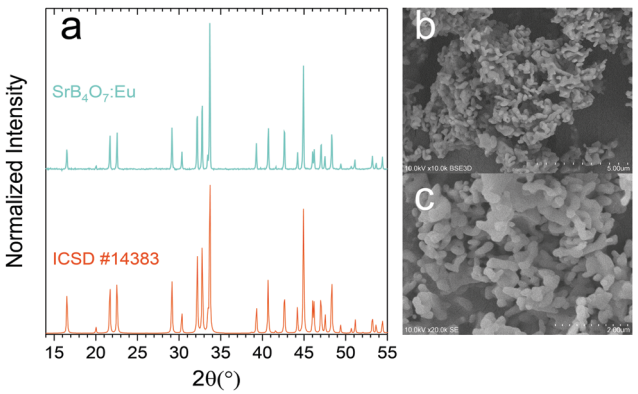

Fig. 2 (a) X-Ray diffraction pattern of SrB_4O_7 containing 3% of Eu^{2+} and prepared in an air atmosphere. (b and c) SEM images of the SrB_4O_7:Eu^{2+} powder, taken at different magnifications (b - 5 μm scale bar; c - 2 μm scale bar).

For thermometric purposes, we measured the temperature dependence of the PL spectra (Fig. 4a) and decay traces of Eu^{2+} luminescence (Fig. 4b and c) in the *T*-range of 11–600 K. With the increasing temperature, three narrow lines, blue-shifted in respect to the $^6P_{7/2} \rightarrow {}^8S_{7/2}$ transition emerge (see Fig. 4a and Fig. S1 in ESI†). These three higher-energy components result from the thermally populated Stark sub-levels of the $^6P_{7/2}$ manifold,[8] *i.e.*, from the $^6P_{7/2} \rightarrow {}^8S_{7/2}$ intra-configurational transition of Eu^{2+}. Their spectral positions are in good agreement with the theoretically calculated splitting of the $^6P_{7/2}$ state into four Stark sub-levels, for the C_s symmetry.[33] With increasing temperature, the $4f^65d^1 \rightarrow 4f^7$ broadband component suddenly appears and dominates the spectrum above 60 K. This obviously reflects the thermal population of the $5d_1$ level, as discussed in the Introduction. Despite the increasing intensity of the inter-configurational emission, the $^6P_{7/2} \rightarrow {}^8S_{7/2}$ luminescence is clearly visible even up to ≈600 K, being potentially useful for luminescence thermometry applications.

Apart from the PL spectrum, the decay kinetics of Eu^{2+} emission also reveal a significant temperature dependence. Fig. 4b and c present decay traces of Eu^{2+} luminescence, recorded in the 11–600 K range. As the temperature increases, the decay time drastically shortens. Such characteristics of the luminescence kinetics are also in accordance with the energy scheme of Eu^{2+} presented in Fig. 1b. At the lowest temperature (11 K), the spin- and parity-forbidden $^6P_{7/2} \rightarrow {}^8S_{7/2}$ emission dominates, and this implicates the longest decay time. With increasing temperature, the contribution from the 5d → 4f parity-allowed (but spin-forbidden) transition systematically increases, shortening the decay time. Meijerink *et al.*[8] have shown that the lowest level of the $4f^65d^1$ excited configuration lies ∼130 cm^{-1} above the lowest excited Stark sub-level of $^6P_{7/2}$

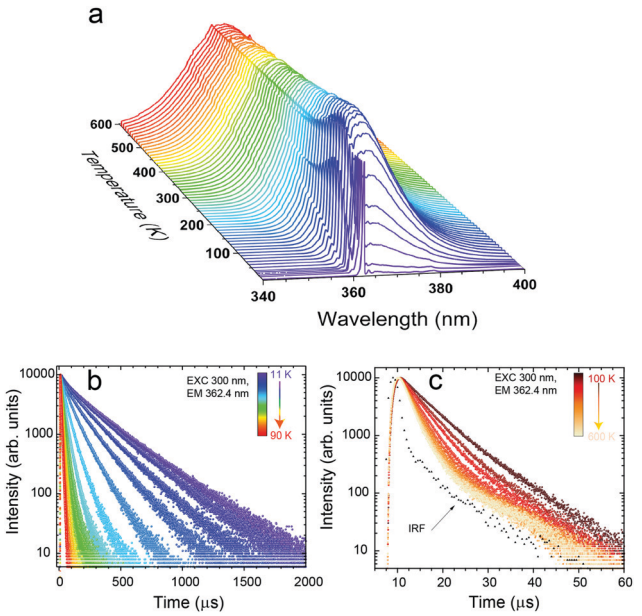

Fig. 4 (a) Normalized (at 362.4 nm) temperature-dependent luminescence spectra of the SrB_4O_7:Eu^{2+} material, measured in the 11–600 K range upon excitation at 300 nm. Temperature-dependent decay traces of Eu^{2+} luminescence, recorded in the range (b) 11–90 K and (c) 100–600 K range.

of Eu^{2+}. Due to the mentioned small energy difference, efficient thermal coupling of the $4f^6 5d^1$ and the $4f^7$ ($^6P_{7/2}$) states can occur even at low temperatures. Note that both the intra-configurational $^6P_{7/2} \rightarrow {}^8S_{7/2}$ and the inter-configurational $4f^6 5d^1 \rightarrow {}^8S_{7/2}$ emission bands have the same terminal (ground) level, and the corresponding transitions start from the thermally coupled states.[7,34] In such a system, with the ΔE representing the energy difference between the involved levels, the rates of transitions from the levels being $p_{2\rightarrow1}$ (the 4f → 4f in the discussed system) and $p_{3\rightarrow1}$ (5d → 4f), the luminescence decay time (τ), at temperature T is well described by eqn (1):[34–37]

$$p = \frac{1}{\tau} = p_{2\rightarrow1}\frac{e^{\Delta E/kT}}{1+e^{\Delta E/kT}} + p_{3\rightarrow1}\frac{1}{1+e^{\Delta E/kT}} \quad (1)$$

The luminescence decay curves recorded at higher temperature values presented in Fig. 4c (having a dominant contribution of the 5d → 4f emission), exhibit nearly a single exponential behavior, although the perfect fits required the use of a two-exponential function, eqn (2):[38]

$$I(t) = A_0 + \sum_{i=1}^{n} \alpha_i \exp(-t/\tau_i) \quad (2)$$

where t_1 and t_2 are the decay time constants, τ_i are amplitudes of the relative components at time $t = 0$ and A_0 is the background intensity.

Thus, for temperature sensing applications, the average decay time, $\bar{\tau}$ calculated according to eqn (3):[38]

$$\bar{\tau} = \frac{\int I(t)\cdot t\,dt}{\int I(t)\cdot dt} \quad (3)$$

was used as a thermometric parameter.

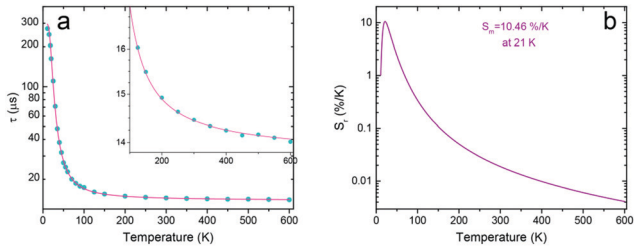

Fig. 5 (a) Average decay time $\bar{\tau}$ (eqn (3)) of SrB_4O_7:Eu^{2+} under 300 nm excitation and monitored at 362.4 nm. (b) Calculated relative thermal sensitivity of the investigated phosphor.

The most potent changes of the luminescence decay time occur between ≈10 and 100 K, when it decreases from ~300 μs to ~14 μs, see Fig. 5a. At higher temperature values, the decay time further shortens monotonically, proving the growing contribution of the allowed 5d → 4f transition to the total emission of Eu^{2+}.

3.3. Luminescence decay time as a thermometric parameter

One of the most important parameters for characterizing and comparing the performance of a luminescence thermometer with other thermometers is its relative thermal sensitivity (S_r). Using the luminescence decay time as a thermometric parameter, S_r was calculated according to eqn (4):[39]

$$S_r = \frac{1}{\tau}\left|\frac{\partial\tau}{\partial T}\right|. \quad (4)$$

Applying the luminescence decay time mode, the SrB_4O_7:Eu thermometer shows the maximal relative thermal sensitivity, S_m = 10.46%/K at 21 K. This is one of the highest relative thermal sensitivities reported, using the luminescence decay time as a thermometric parameter. At higher temperature values, the relative sensitivity decreases rapidly and monotonously. Yet, up to 600 K, the decay time may serve as a reliable thermometric parameter, which makes the operating range as broad as 11–600 K.

3.4. Luminescence intensity ratio as a thermometric parameter

The temperature-induced changes in the luminescence spectra are evidently attractive for luminescence thermometry, as well (see Fig. 4a). To determine the thermometric parameters, we chose four different spectral areas denoted as A1, A2, A3 (4f → 4f narrow emission lines), and A4 (5d → 4f broad emission band) presented in Fig. 6. It should be noted that the two emissions discussed above, *i.e.*, 5d → 4f and the $^6P_{7/2} \rightarrow {}^8S_{7/2}$ (4f → 4f) superimpose strongly, which poses the question about the possibility of separating the corresponding, spectrally overlapping bands. Moreover, with increasing temperature, the number of narrow lines clearly contributes to the total luminescence changes, as the number of vibronic features and those related to the transitions from the thermally-populated Stark sub-levels change in the PL spectrum. This can be seen in Fig. 6a.

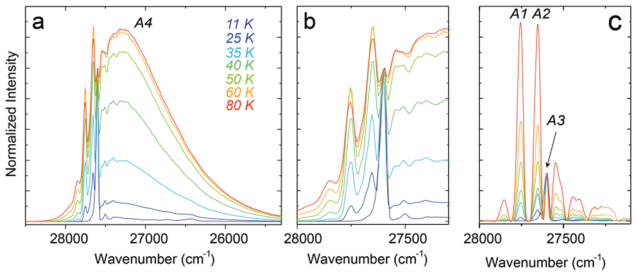

Fig. 6 (a) Temperature-dependent spectra of the SrB_4O_7:Eu^{2+} material in the T-range of 11–80 K and (b) the magnified part of the A1–A3 lines used for Δ parameter determination, (c) presents the spectra after subtracting the broadband fraction related to the 5d → 4f transition.

To calculate the intensities of the individual PL constituents, we separated the broad feature (band), corresponding to the 5d → 4f transition (A4, Fig. 6b), in order to extract the narrow-line components from the PL spectrum (A1–A3, Fig. 6c). For clarity and reproducibility, the applied procedure is depicted in Fig. S2a–c (ESI†), for representative temperature values. All the calculated values of the integrated areas are presented in Fig. S3 (ESI†). Consequently, the thermometric parameters Δ, were calculated for 5 different luminescence intensity ratios. Three of them (Δ_1, Δ_2, and Δ_3) involved the ratio between the broadband and one of the narrow lines. The next two fractions (Δ_4 and Δ_5) represent the intensity ratios between the narrow lines. Thus, the Δ parameters were calculated according to eqn (5):

$$\Delta_1 = \frac{A4}{A1}, \quad \Delta_2 = \frac{A4}{A2}, \quad \Delta_3 = \frac{A4}{A3}, \quad \Delta_4 = \frac{A1}{A3}, \quad \Delta_5 = \frac{A2}{A3}, \quad (5)$$

The thermal evolution of the Δ_{1-5} parameters is presented in Fig. 7a. The errors in the determination Δ_{1-5} were calculated using eqn (6):[40]

$$\delta\Delta_x = \sqrt{\left(\frac{\delta I_1}{I_1}\right)^2 + \left(\frac{\delta I_2}{I_2}\right)^2} \cdot \Delta_x, \quad (6)$$

where I_1 and I_2 are the integrated intensities of two corresponding bands (A1–A5), and $\delta I_i/I_i$ (i = 1, 2) values are estimated by calculating the signal-to-noise values.[40]

The temperature dependence of the thermometric parameters Δ_{1-5} was successfully fitted using empirical functions, *i.e.*, 3th-order polynomials because the Boltzmann function did not give good fits. We will return to this observation in the Discussion section. Table S1 (ESI†) presents the fitting parameters for each of the Δ_{1-5} thermometric parameters. The relative thermal sensitivities were calculated using eqn (3), where τ is replaced by Δ. Fig. 7b presents the calculated S_r values for each investigated Δ parameter. For S_{r4}, an unprecedentedly high value of the maximal relative sensitivity, S_{m4} = 22.60% K^{-1} at 16.5 K, was obtained. To the best of our knowledge, this is the best-reported value so far for inorganic materials doped with lanthanide ions. It should also be noted that for each thermometric parameter used, the calculated relative sensitivity is virtually always greater than 1% K^{-1}, within the entire operating T-range. Importantly, also for the other Δ parameters, the obtained S_m values are very high within the cryogenic T-range, (see Fig. 7b). It is worth noting that for Δ_1 and Δ_2 parameters the S_r values increase with temperature elevation, whereas for the Δ_3–Δ_5 ones the S_r values decrease, as clearly shown in Fig. 7b. Hence, utilizing the developed optical thermometer, the temperature of the system can be monitored in a very broad range, with high thermal sensitivities, better than 1% K^{-1} over the entire operating T-range.

The high values of relative thermal sensitivities are accompanied with high thermal resolutions (reaching even 10^{-3} K in the cryogenic T-range), *i.e.*, small uncertainty values (δT, Fig. 7c) calculated using eqn (7):[40]

$$\delta T = \frac{1}{S_r} \cdot \frac{\delta\Delta}{\Delta} \quad (7)$$

where $\delta\Delta/\Delta$ stands for the error in the determination of Δ parameter (see eqn (6)). Fig. 7c presents the δT for all investigated Δ parameters. It is worth noting, that all δT values are in the 0.001–0.1 K range up to ≈100 K, which is very beneficial for various thermometric applications.

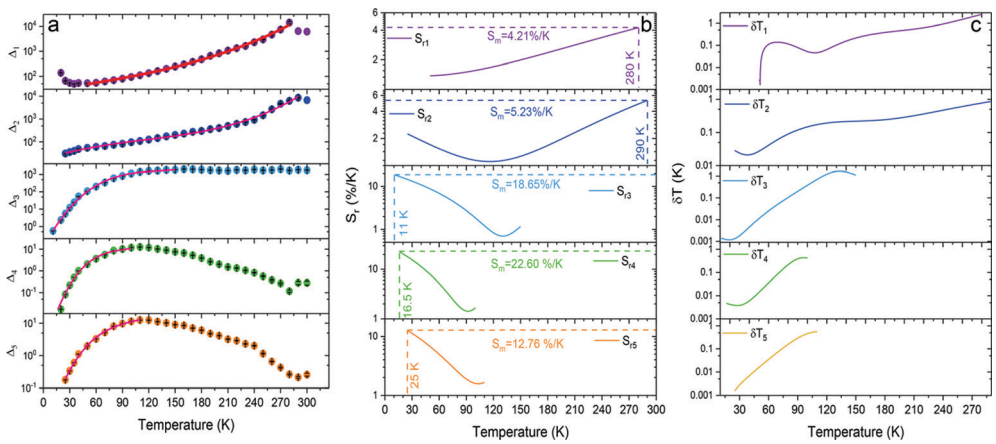

Fig. 7 (a) Thermal evolution of Δ parameters for the SrB_4O_7:Eu^{2+} phosphor, (b) its relative thermal sensitivities, and (c) corresponding temperature uncertainties.

4. Discussion

It is notable that the maximal tvalues of the relative thermal sensitivities (S_m) are very high both for the luminescence lifetimes ($S_m \approx 10.5\%\ K^{-1}$) and for the band intensity ratios ($S_m \approx 22.6\%\ K^{-1}$). The highest S_r values can be achieved in the T-range of 11–50 K. However, the operating range of the developed temperature sensor material – $SrB_4O_7:Eu^{2+}$ – spans the 11–600 K range, using different sensing modes – lifetimes and intensity ratios. This makes the luminescent thermometer both a wide-range and extraordinarily sensitive tool. Its capability to work in different modes and to operate with multi-parameters makes it a universal sensor for thermometric purposes.

Table 1 compares the most important optical thermometry figure of merits, of the developed sensor $SrB_4O_7:Eu^{2+}$ with other high-performance inorganic, luminescent thermometers reported in the literature. Recently, Marciniak *et al.*[41] presented an original strategy to develop luminescence thermometers based on a reversible phase transition and achieved S_m = 11.8% K^{-1} at 295 K (that is, around room temperature). In turn, the inorganic optical thermometer developed in this work is currently the leader in terms of thermal sensitivity in the cryogenic T-range.

As we mentioned in the Introduction part, achieving a broad operating T-range combined with high relative sensitivity is a great challenge in the field of luminescence thermometry. In this paper, we showed that the Eu^{2+} luminescence in the strontium borate host matrix may fulfill the most important requirements of such thermometers. Thermal coupling of the excited states, the $^6P_{7/2}$ level of the $4f^7$ configuration, and the lowest level of the $4f^65d^1$ configuration may offer both spectacular sensitivity and a wide operating range, spanning from cryogenic to at least 600 K. Since the energy of the $^6P_{7/2}$ level is basically fixed and independent of the host, the only way to design such thermometers is to maintain the energy of the $4f^65d^1$ excited state slightly above the $^6P_{7/2}$ emitting level.

The energy of the lowest state of the $4f^65d^1$ excited configuration is defined by the crystal-field splitting of this configuration, as well as by the ionicity of the chemical bonding of Eu^{2+}. These bonds should be strongly ionic to shift the entire $4f^65d^1$ configuration to higher energies. Then, the crystal-field splitting of the configuration should be as low as possible, to avoid shifting the lowest-energy $4f^65d^1$ level too much downward. These requirements are in some sense contradictory since the ionic bonds exert a fairly high crystal-field strength. Yet, what may help is the introduction of the Eu^{2+} ion into a large site with a high coordination number of ligands that readily form ionic bonds. Apparently, these basic requirements are quite well-fulfilled in the SrB_4O_7:Eu phosphor. In order to shift the maximal relative sensitivity of the sensor to a higher temperature region, the gap between the lowest $4f^65d^1$ level and the $^6P_{7/2}$ level below it should be greater than 130 cm^{-1} in $SrB_4O_7:Eu^{2+}$.

We would like to emphasize, yet, the difference (from the luminescence thermometry point of view) between the Eu^{2+} emission used here and the previously published properties of Pr^{3+} emission.[20–22] In thermometers using the latter dopant, emissions from the non-thermally-coupled levels were exploited and thermal quenching of such emissions was inherently utilized to get a high-performance sensor. This necessarily degraded the emission intensity deteriorating their thermal resolution (by decreasing the signal-to-noise ratio). On the contrary, in the case of the $SrB_4O_7:Eu^{2+}$ sensor material, the emission of Eu^{2+} is not thermally quenched in the classical sense – the energy gained by the ion is not lost non-radiatively

Table 1 Thermometric performance of illustrative examples of the most sensitive, inorganic-based luminescence thermometers

Material	Measured parameter	S_m (% K^{-1})	T_m (K)	T-range (K)	Equation type for Δ or τ-fitting	Ref.
$SrB_4O_7:Eu^{2+}$	τ	10.47	21	11–600	Three-level system equation[36]	This work
	Δ_1	4.21	280	50–280	Polynomial equation	
	Δ_2	5.23	290	25–290		
	Δ_3	18.65	11	11–150		
	Δ_4	22.60	16.5	16.5–100		
	Δ_5	12.76	25	25–110		
$LiYO_2:Eu^{3+}$	Δ	11.80	295	263–376[a]	From experimental data	41
$Sr_2Ge_{0.75}Si_{0.25}O_4:Pr^{3+}$	Δ	9.20	65	18–600	Mott–Seitz equation	21
$Sr_2GeO_4:Pr^{3+}$	Δ	9.00	22	17–600	Mott–Seitz equation	20
$YVO_4:Nd^{3+}$	Δ	9.00	123	123–873	Boltzmann equation	46
$LaF_3:Er^{3+},Yb^{3+}$	Δ	6.61	15	15–105	Mott–Seitz equation	47
Bi_2MoO_6: Er^{3+},Tm^{3+},Yb^{3+}	Δ	5.50	293	293–623	Polynomial equation	48
$Y_2Ti_2O_7:Pr^{3+}$	Δ	5.25	289	289–573	Semi-empirical equation	49
$SrTiO_3:Lu^{3+}$	Δ	4.60	200	120–290[a]	From experimental data	50
$ZnGa_2O_4:Cr^{3+}$	Δ	2.80	310	77–450	Boltzmann equation	51
$Bi_2SiO_5:Yb^{3+},Tm^{3+}@SiO_2$	Δ	2.60	280	400–800	Boltzmann equation	52
$TiO_2:Sm^{3+}$	Δ	10.54	330	298–383[a]	Not reported	53
	τ	10.15	339			
$Al_2O_3:Sm^{2+}$	Δ	4.80	298	298–648	Boltzmann equation	54
	τ	1.20	531	100–620		
$SrTiO_3:Tb^{3+}$	τ	8.83	180	10–230	From experimental data	50
$SrB_4O_7:Sm^{2+}$	τ	3.36	550	300–673	Boltzmann equation	55
$Y_2SiO_5:Pr^{3+}$	τ	2.67	417	11–500	Double-barrier equation	56
$GAG:Mn^{3+},Mn^{4+}$	τ	2.08	249	123–350[a]	Mott–Seitz equation	57

[a] Eestimated based on figures in given references.

but is split between the two emitting levels of the dopant, instead. This is an important advantage, as the overall emission intensity is hardly dependent on temperature, with a respective reduction in the uncertainty of the measured temperature.

At first, it is surprising that the thermometric parameters based on luminescence intensity ratio (Fig. 7a) could not be effectively fitted using the Boltzmann function, despite the $^6P_{7/2}$ and the $4f^65d^1$ emitting levels are obviously thermally coupled. In the earlier literature, one may find examples of similar divergence from anticipations.[42,43] Such a problem is typically encountered when luminescence intensity ratio in a *wide range* of temperature is analyzed or complex relaxation processes between (or from) the thermally coupled levels take place.[42,44] Such circumstances seem to exist in the SrB_4O_7:Eu^{2+} phosphor. The decay time of the 5d → 4f luminescence presents measurable (and useful for temperature sensing) changes from 11 to 600 K, while the 5d → 4f/4f → 4f luminescence intensity ratio appeared useful as thermometric parameter merely up to about 280 K. Detailed understanding of all aspects of the reasons of the non-Boltzmann dependence of the ratio of the emissions would require much more comprehensive examination of the phosphor. Possibly, more thorough computational exploration of deconvolution of the experimental spectra into the numerous components would be needed.

Finally, we note that the Eu^{2+} the characteristics of the luminescence of the SrB_4O_7:Eu^{2+} phosphor presents some similarity with emission of Cr^{3+} in some hosts. The latter ion shows interesting thermometric properties when its thermally coupled $^4T_2$ and ^2E excited states are employed.[43,45] And also in this case this is the crystal field which plays an important role. When it is strong enough to lift the $^4T_2$ level above the ^2E one, the Boltzmann distribution between them defines the thermometric performance of the selected phosphor. Yet, also for Cr^{3+}, the Boltzmann law is obeyed over a limited range of temperature and in wide ranges it is not,[43] exactly as for Eu^{2+}. Thus, the physics defining the SrB_4O_7:Eu^{2+} phosphor thermometric performance and standing behind the Cr^{3+} activated luminescence thermometers are fairly similar.

5. Conclusions

Here, we have shown that the selection of an appropriate host matrix (in our case SrB_4O_7) embedded with the desired, optically active divalent lanthanide ions (in this case Eu^{2+}) is essential for the development of highly sensitive optical thermometers. The decisive role in designing such temperature sensors is an interplay between the inter- and intra-configurations transitions within the activator ion, where the relative energy difference of the corresponding excited states is crucial to achieving unprecedentedly high thermal sensitivity and great resolution of the final luminescent thermometer. In this work, it was found that the luminescence properties of the investigated SrB_4O_7:Eu^{2+} phosphor are very promising for thermometric purposes. Its emission spectra, as well as the decay kinetics, are strongly temperature-dependent. In the cryogenic temperature range, below ≈20 K, the emission results mainly from the intra-configurational $^6P_{7/2}$ → $^8S_{7/2}$ transition, while with increasing temperature, the broadband luminescence resulting from the inter-configurational 5d → 4f transition begins to appear, and increasingly contributes to the overall emission intensity. This results from the thermal coupling of the two emitting levels separated only by about 130 cm^{-1}. Another consequence of this thermal coupling between the excited $^6P_{7/2}$ and the lowest $4f^65d^1$ levels is the strong temperature dependence of the luminescence decay time, which significantly shortens with increasing temperature. Altogether, the SrB_4O_7:Eu^{2+} phosphor presents very attractive properties for thermometric purposes. Its broad operating range in ratiometric mode spans the 11–280 K range, and its maximal relative sensitivities vary from ≈4 to above 22% K^{-1} (depending on the Δ parameter used). Using the luminescence decay time as a thermometric parameter the operating range is even broader, namely 11–600 K, and the maximal relative thermal sensitivity was found to reach 10.46% K^{-1}, which is one of the highest values ever reported for relative sensitivity based on a luminescence decay time. Importantly, the high sensitivity values are in line with great thermal resolutions, which reach even 10^{-3} K in the cryogenic *T*-range. This paper proves that Eu^{2+} luminescence may offer much more for thermometry than previously thought.

Author contributions

The manuscript was written through the contributions of all authors. All authors have given approval to the final version of the manuscript.

Conflicts of interest

There are no conflicts to declare.

Acknowledgements

This research was supported by the Polish National Science Centre (NCN) under grant #UMO 2018/29/B/ST5/00420. Publication partially financed by the program ''Excellence Initiative – Research University''.

References

1 M. D. Dramićanin, *J. Appl. Phys.*, 2020, **128**, 040902.
2 C. D. S. Brites, S. Balabhadra and L. D. Carlos, *Adv. Opt. Mater.*, 2019, **7**, 1801239.
3 Y. Gao, Y. Cheng, T. Hu, Z. Ji, H. Lin, J. Xu and Y. Wang, *J. Mater. Chem. C*, 2018, **6**, 11178–11183.
4 M. Runowski, P. Woźny, S. Lis, V. Lavín and I. R. Martín, *Adv. Mater. Technol.*, 2020, 1901091.
5 M. A. Hernández-Rodríguez, K. Kamada, A. Yoshikawa, J. E. Muñoz-Santiuste, A. Casasnovas-Melián, I. R. Martín,

U. R. Rodríguez-Mendoza and V. Lavín, *J. Alloys Compd.*, 2021, 161188.
6 L. Marciniak, K. Elzbieciak-Piecka, K. Kniec and A. Bednarkiewicz, *Chem. Eng. J.*, 2020, **388**, 124347.
7 G. Blasse and B. Grabbmaier, *Luminescent Materials*, Springer-Verlag, Berlin Heidelberg, 1994.
8 A. Meijerink, J. Nuyten and G. Blasse, *J. Lumin.*, 1989, **44**, 19–31.
9 P. Dorenbos, *J. Lumin.*, 2013, **135**, 93–104.
10 J. G. Bunzli and S. V. Eliseeva, *Springer Ser. Fluoresc.*, 2011, 1–45.
11 M. Suta and C. Wickleder, *J. Lumin.*, 2019, **210**, 210–238.
12 M. Suta, F. Lavoie-Cardinal and C. Wickleder, *Angew. Chem., Int. Ed.*, 2020, **59**, 10949–10954.
13 F. Datchi, R. LeToullec and P. Loubeyre, *J. Appl. Phys.*, 1997, **81**, 3333–3339.
14 T. Zheng, M. Runowski, P. Woźny, S. Lis and V. Lavín, *J. Mater. Chem. C*, 2020, **8**, 4810–4817.
15 G. Blasse, G. J. Dirksen and A. Meijerink, *Chem. Phys. Lett.*, 1990, **167**, 41–44.
16 P. Solarz, J. Komar, M. Głowacki, M. Berkowski and W. Ryba-Romanowski, *RSC Adv.*, 2017, **7**, 21085–21092.
17 W. Xu and J. R. Peterson, *J. Alloys Compd.*, 1997, **249**, 213–216.
18 M. De Jong, A. Meijerink, R. A. Gordon, Z. Barandiarán and L. Seijo, *J. Phys. Chem. C*, 2014, **118**, 9696–9705.
19 M. De Jong, A. Meijerink, Z. Barandiarán and L. Seijo, *J. Phys. Chem. C*, 2014, **118**, 17932–17939.
20 C. D. S. Brites, K. Fiaczyk, J. F. C. B. Ramalho, M. Sójka, L. D. Carlos and E. Zych, *Adv. Opt. Mater.*, 2018, 1701318.
21 M. Sójka, J. F. C. B. Ramalho, C. D. S. Brites, K. Fiaczyk, L. D. Carlos and E. Zych, *Adv. Opt. Mater.*, 2019, **7**, 1901102.
22 M. Sójka, C. D. S. Brites, L. D. Carlos and E. Zych, *J. Mater. Chem. C*, 2020, **8**, 10086–10097.
23 P. Bolek, J. Zeler, C. D. S. Brites, J. Trojan-Piegza, L. D. Carlos and E. Zych, *Chem. Eng. J.*, 2021, **421**, 129764.
24 T. Zheng, M. Sójka, M. Runowski, P. Woźny, S. Lis and E. Zych, *Adv. Opt. Mater.*, 2021, **9**, 2101507.
25 Y. Pan, X. Xie, Q. Huang, C. Gao, Y. Wang, L. Wang, B. Yang, H. Su, L. Huang and W. Huang, *Adv. Mater.*, 2018, **30**, 3–8.
26 L. Zhou, P. Du and L. Li, *Sci. Rep.*, 2020, **10**, 1–11.
27 D. Stefańska, M. Stefanski and P. J. Dereń, *J. Alloys Compd.*, 2021, **863**, 1–7.
28 R. Zhou, C. Liu, L. Lin, Y. Huang and H. Liang, *Chem. Eng. J.*, 2019, **369**, 376–385.
29 R. Zhou, L. Lin, H. Zhao, T. Deng and J. Li, *Mater. Chem. Front.*, 2021, **5**, 6071–6081.
30 D. Dutczak, T. Jüstel, C. Ronda and A. Meijerink, *Phys. Chem. Chem. Phys.*, 2015, **17**, 15236–15249.
31 P. Solarz, M. Karbowiak, M. Głowacki, M. Berkowski, R. Diduszko and W. Ryba-Romanowski, *J. Alloys Compd.*, 2016, **661**, 419–427.
32 I. V. Berezovskaya, V. P. Dotsenko, A. S. Voloshinovskii and S. S. Smola, *Chem. Phys. Lett.*, 2013, **585**, 11–14.
33 J. G. Bunzli and S. V. Eliseeva, *Springer Ser. Fluoresc.*, 2011, 1–45.
34 K. Fiaczyk, A. J. Wojtowicz and E. Zych, *J. Phys. Chem. C*, 2015, **119**, 5026–5032.
35 B. Di Bartolo and R. Summitt, *Phys. Today*, 1970, **23**, 105–107.
36 G. A. M. Dalhoeven and G. Blasse, *J. Solid State Chem.*, 1981, **39**, 35–38.
37 P. Kisliuk and C. A. Moore, *Phys. Rev.*, 1967, **160**, 307–312.
38 J. R. Lakowicz, *Principles of Fluorescence Spectroscopy*, Springer, US, Boston, MA, 2006, pp. 1–26.
39 C. D. S. Brites, P. P. Lima, N. J. O. Silva, A. Millán, V. S. Amaral, F. Palacio and L. D. Carlos, *Nanoscale*, 2012, **4**, 4799.
40 C. D. S. Brites, A. Millán and L. D. Carlos, *Handbook on the Physics and Chemistry of Rare Earths*, 2016, vol. 49, pp. 339–427.
41 L. Marciniak, W. Piotrowski, M. Szalkowski, V. Kinzhybalo, M. Drozd, M. Dramicanin and A. Bednarkiewicz, *Chem. Eng. J.*, 2022, **427**, 131941.
42 R. G. Geitenbeek, H. W. De Wijn and A. Meijerink, *Phys. Rev. Appl.*, 2018, **10**, 1.
43 M. Back, J. Ueda, M. G. Brik and S. Tanabe, *ACS Appl. Mater. Interfaces*, 2020, **12**, 38325–38332.
44 M. Suta and A. Meijerink, *Adv. Theory Simul.*, 2020, **3**, 1–32.
45 M. Back, J. Ueda, H. Nambu, M. Fujita, A. Yamamoto, H. Yoshida, H. Tanaka, M. G. Brik and S. Tanabe, *Adv. Opt. Mater.*, 2021, **9**, 1–11.
46 A. A. Kalinichev, M. A. Kurochkin, E. V. Golyeva, A. V. Kurochkin, E. Lähderanta, M. D. Mikhailov and I. E. Kolesnikov, *J. Lumin.*, 2018, **195**, 61–66.
47 A. M. Kaczmarek, M. K. Kaczmarek and R. Van Deun, *Nanoscale*, 2019, **11**, 833–837.
48 T. Zheng, M. Runowski, N. Stopikowska, M. Skwierczyńska, S. Lis, P. Du and L. Luo, *J. Alloys Compd.*, 2021, **890**, 161830.
49 R. Lei, X. Luo, Z. Yuan, H. Wang, F. Huang, D. Deng and S. Xu, *J. Lumin.*, 2019, **205**, 440–445.
50 W. Piotrowski, M. Kuchowicz, M. Dramićanin and L. Marciniak, *Chem. Eng. J.*, 2022, **428**, 131165.
51 J. Ueda, M. Back, M. G. Brik, Y. Zhuang, M. Grinberg and S. Tanabe, *Opt. Mater.*, 2018, **85**, 510–516.
52 E. Casagrande, M. Back, D. Cristofori, D. Cristofori, J. Ueda, S. Tanabe, S. Palazzolo, F. Rizzolio, F. Rizzolio, V. Canzonieri, V. Canzonieri, E. Trave and P. Riello, *J. Mater. Chem. C*, 2020, **8**, 7828–7836.
53 M. D. Dramićanin, Ž. Antić, S. Ćulubrk, S. P. Ahrenkiel and J. M. Nedeljković, *Nanotechnology*, 2014, **25**, 485501.
54 A. Ćirić, S. Stojadinović, Z. Ristić, I. Zeković, S. Kuzman, Ž. Antić and M. D. Dramićanin, *Adv. Mater. Technol.*, 2021, **6**, 1–10.
55 Z. Cao, X. Wei, L. Zhao, Y. Chen and M. Yin, *ACS Appl. Mater. Interfaces*, 2016, **8**, 34546–34551.
56 M. Sójka, M. Runowski, P. Woźny, L. D. Carlos, E. Zych and S. Lis, *J. Mater. Chem. C*, 2021, **9**, 13818–13831.
57 L. Marciniak and K. Trejgis, *J. Mater. Chem. C*, 2018, **6**, 7092–7100.